INTERNATIONAL SOCIETY FOR SOIL MECHANICS AND GEOTECHNICAL ENGINEERING

IS-PORTO 2023
PROCEEDINGS

Evaluation of non-uniformity of sandy soil specimens compacted in the field and laboratory using triaxial tests

Yuichi Tomita[1#], and *Junichi* Koseki[2]

[1]*Tokyu Construction Co., Ltd., Institute of Technology, 3062-1 Tana Chuo-ku Sagamihara-shi Kanagawa, Japan*
(Formerly known as The University of Tokyo)
[2]*The University of Tokyo, Department of Civil Engineering, 7-3-1 Hongo Bunkyo-ku Tokyo, Japan*
[#]*Corresponding author: tomita.yuuichi@tokyu-cnst.co.jp*

ABSTRACT

The strength and deformation characteristics of compacted soils are typically evaluated using triaxial compression tests on specimens that are compacted relatively uniformly in a laboratory. Soil compacted in the field using vibration rollers is nonuniform in the vertical depth direction; this is because the gradient of the dry density and saturation degree in the depth direction of each compaction layer is large, owing to the distribution of the load transmitted from the contact surface. As a quality control method for earth-filling works, nondestructive inspection indices—such as the soil stiffness index— are applied in some cases, and the average value of the nonuniform compaction layers is measured. Further, unsaturated specimens, which were retrieved from the test fill yielded during field compaction tests, and specimens obtained via compaction using the same soil as that in the laboratory were prepared, and then triaxial compression tests were performed. Local displacement transducers were installed to obtain local deformation characteristics, based on the vertical depth of the specimen, which were then compared with the average deformation characteristics of the entire specimen. The results show that the local low-stiffness section significantly affects the overall average; this makes it non-negligible because the specimen compacted in the field is nonuniform. However, because field-compacted soil has a local low-stiffness section near the surface layer compared with laboratory-compacted soil, evaluations based on the nondestructive inspection of the surface layer may result in underestimations.

Keywords: sandy soil; compaction; non-uniformity; local deformation.

1. Introduction

To achieve high-performance filling structures, the design parameters—density, strength, and stiffness—of the filling materials after compaction must be specified using triaxial tests in a laboratory and their quality after construction must be ensured. Recently, in addition to the conventional soil density test in the field, an evaluation method using the California Bearing Ratio and ground reaction coefficient, acceleration response of a vibration roller, and initial shear stiffness coefficient based on the soil stiffness index of a relatively low strain level has been proposed (Tatsuoka et al. 2021), (Moony and Adam 2007), (Heitor et al. 2016).

To investigate the correlation between the soil stiffness index of an unsaturated compacted soil measured in the field and the strength and stiffness obtained via a triaxial compression test on soil compacted in a laboratory under wet/saturated conditions, the authors compared the difference in the strength deformation characteristics between a laboratory-compacted and a field-compacted specimen with the same fill material (Tomita et al. 2021), (Tomita et al. 2022).

Because the strength deformation properties of compacted soils in unsaturated and saturated states are significantly affected by the saturation degree S_r at compaction, in addition to the dry density ρ_d, the effects of the S_r and ρ_d at compaction should be considered to estimate the design parameters based on the strength properties of compacted soils in the field.

In addition, the vibration roller traverses the scattered soil during field compaction; consequently, the load is dispersed downward from above the compaction layer, causing the density distribution in the vertical depth direction to be nonuniform (Fig. 1). These effects must be considered when evaluating the strength–deformation characteristics of compacted soil in fields. Previously, the effect of laboratory-compacting on the liquefaction properties of nonuniform specimens was investigated using triaxial compression tests and particle image velocimetry analysis; the reference point assigned to the specimen was monitored and the porosity ratio and sectional change were evaluated during the undrained shearing of triaxial compression and extension tests using X-ray computed tomography (CT) (Thomson and Wong 2008).

Investigations similar to this are scarce, and evaluation techniques using image analysis are difficult to apply in the evaluation of the deformation characteristics at small strain levels.

Therefore, the effect of local deformation on the initial Young's modulus E_0 (Vertical strain $\Delta\varepsilon_v \approx 0.001\%$) of an entire specimen obtained using a triaxial compression test was examined in this study by installing a local displacement transducer at each vertical depth of
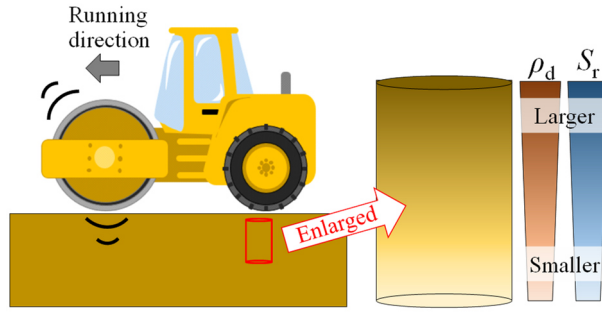
Figure 1. Schematic diagram of nonuniform field-compacted soil.
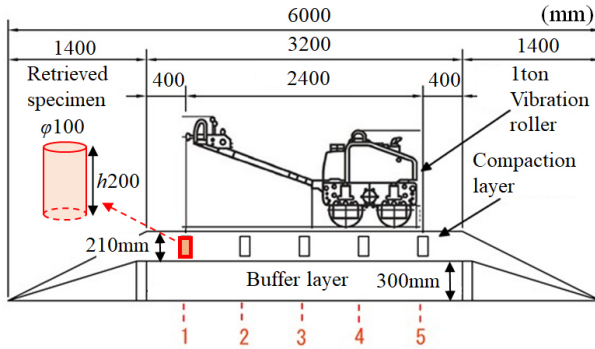
Figure 2. Outline of the test fill and sampling position of the field-compacted specimen.

Figure 3. Compaction condition of the specimens before the triaxial compression tests; ρ_d vs. w graphs.

Table 1. Relative deviation of the upper and lower sections of the specimen to the average dry density

Compaction method		Laboratory			Field
Compaction energy level		$4.5E_c$	$1.0E_c$	$0.2E_c$	—
Relative deviation*	**Upper section**	-1.1%	-0.46%	-0.33%	2.0%
	Lower section	0.55%	0.15%	0.06%	-2.0%

* Relative deviation: $[\rho_d / (\rho_d)_{ave} - 1] \times 100$ (%)

the specimen compacted in the field and laboratory, respectively.

2. Specimen preparation

Sandy soil (Inagi sand) that featured a maximum grain size $D_{max} = 2.0$ mm, mean grain size $D_{50} = 0.25$ mm, and fines content $F_c = 8.4\%$ was used as the fill material. The optimum water content determined using the compaction test is $w_{opt} = 14.2\%$, the maximum dry density $(\rho_d)_{max} = 1.684 \text{g/cm}^3$, and the optimum degree of saturation $(S_r)_{opt} = 64.1\%$. Here, the $(S_r)_{opt}$ is defined as S_r when the $(\rho_d)_{max}$ is obtained for a specified compaction energy level (standard Proctor, $1.0E_c$).

Test fills for full-scale compaction tests were constructed for the specimens compacted in the field (Tomita et al. 2021), and samples ($\varphi100$ mm × $h200$ mm) with negligible disturbance were retrieved via soil block sampling (JGS1231). Each test fill was constructed using a fill material in one layer (layer thickness $t = 0.21$ m after compaction) of a steel earth vessel measuring 3.2 m (length) × 2.0 m (width) by evenly passing a 1-ton hand guide-type vibration roller with a vibratory force of 11.8 kN, mass 605 kg, and width 0.7 m (Fig. 2). Test fills with varying water-content conditions were prepared using this method. Specimens were then retrieved and compared with the field-compacted specimens using the same measurement procedure as that used on the compacted specimens in the laboratory.

The specimens were then compacted in the laboratory using the same fill material as that used in the test fill. Subsequently, they were prepared as uniformly-compacted specimens and placed in a steel mould
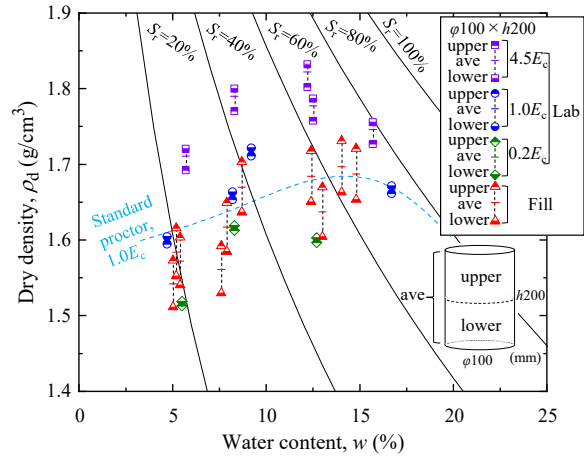
measuring $\varphi100$ mm × $h200$ mm in five layers. The compaction energy levels were 0.2, 1.0, and $4.5E_c$ (Tomita et al. 2021).

Fig. 3 shows the compacted state (ρ_d vs. w) of the specimen before the triaxial compression test. The field-compacted specimens were retrieved from the test fill, whereas the laboratory-compacted specimens were controlled by the compaction energy level. Compaction curves were then obtained based on a laboratory compaction curve (Standard Proctor), where the plot of the respective specimens in the figure (w, ρ_d) shows the total average of the specimens measured after preparation. The local dry density of the compacted specimen was then measured to determine the dry density of the upper and lower sections of the specimen. The relative deviation $[\rho_d/(\rho_d)_{ave} - 1]$ of the local dry density to the average dry density $(\rho_d)_{ave}$ is listed in Table 1 for each compaction method. Because ρ_d at the upper and lower sections of each specimen could not be measured during the triaxial compression test, ρ_d was estimated using the relative deviation $[\rho_d/(\rho_d)_{ave}-1]$ and average dry density $(\rho_d)_{ave}$. This estimation method assumes that w in the upper and lower sections of the specimen is the same as the overall average.

3. Testing procedure

Fig. 4 shows the triaxial compression test equipment. The specimens were self-standing in an unsaturated state, isotropically consolidated at a rate of less than 1 kPa/min
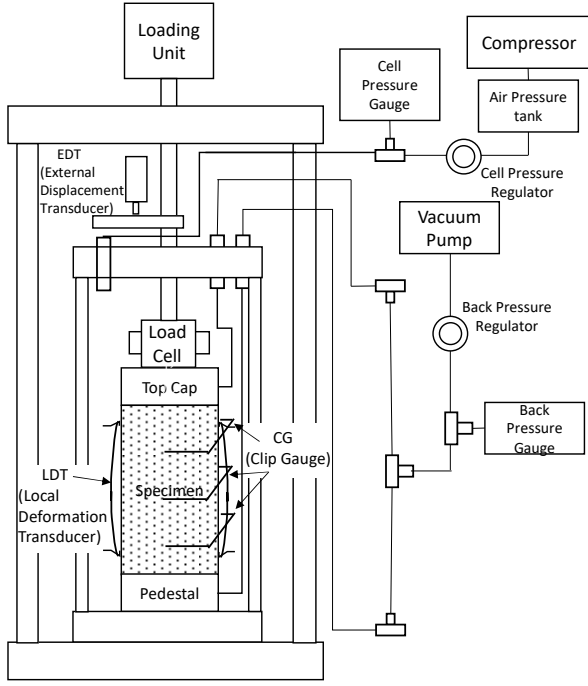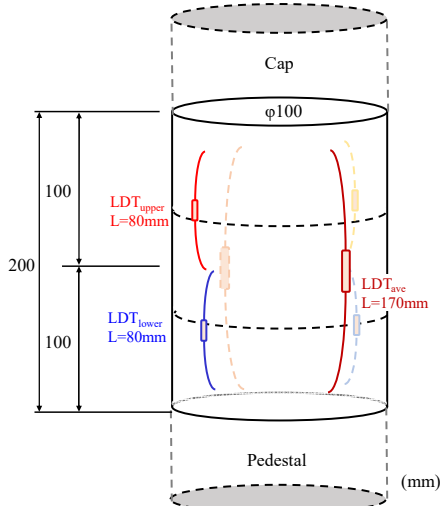
Figure 4. Triaxial apparatus.

Figure 5. Arrangement of the vertical local displacement transducers.

from a ground stress ($p_{net} = (\sigma_{vnet} + 2\sigma_{hnet})/3$) of 10 to 50 kPa, and then monotonically vertically loaded at a rate of 0.02%/min with a fixed ground horizontal stress σ_{hnet}. The vertical strain ε_v was measured as the average strain of the specimen using two local displacement transducers (LDT$_{ave}$: $L = 170$ mm) placed at both ends of the diameter of the specimen to eliminate the bedding error (Goto et al. 1991). Furthermore, to investigate the difference in the deformation properties between the upper and lower sections of the specimen, small local displacement transducers (LDT$_{upper}$, LDT$_{lower}$: $L = 80$ mm) were installed in a 2×2 configuration to avoid the appearance of specimen end faces in the upper and lower halves.

4. Results and discussion

The results of the triaxial compression tests of the specimens under the ρ_d and S_r conditions shown in Fig. 3 are based on the data on the local displacement
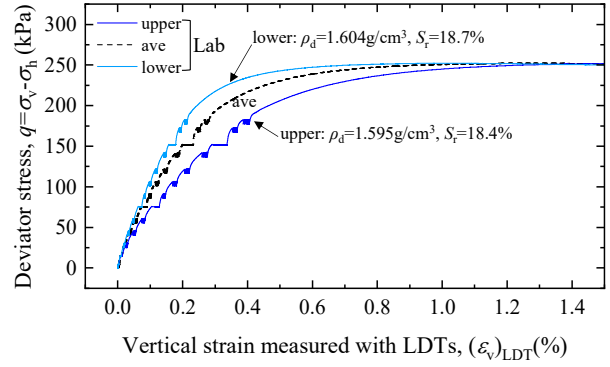

Figure 6. Stress–strain relationships of the laboratory-compacted specimen.
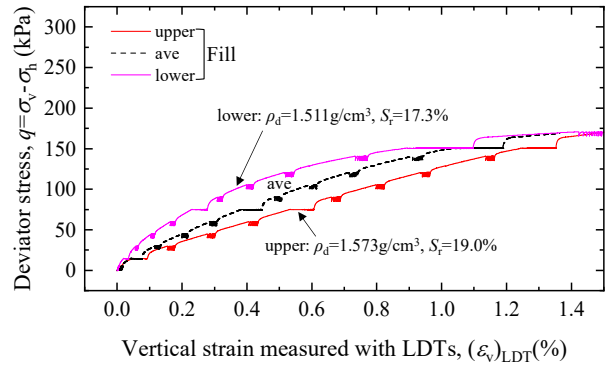

Figure 7. Stress–strain relationships of a field-compacted specimen.

transducers for each part corresponding to the upper section, lower section, and average of the specimens. The deviator stress q was obtained from a common load cell.

4.1. Stress–strain relationships

Fig. 6 shows an example of the stress–strain relationship of a specimen compacted in the laboratory. Although the measurements could not be obtained up to a distinct peak, the deviator stress q of each curve coincided at approximately $\varepsilon_v = 1.5\%$. Additionally, the secant stiffness before the peak in the lower section is higher than that in the upper section. The secant Young's modulus, E_{50}, was obtained as 56.1 MPa and 101.5 MPa in the upper and lower sections of the specimen, respectively, based on the Young's modulus at 50% of the maximum deviator stress. Because the compaction energy level of this specimen is $1.0E_c$ and the lower section exhibits a slightly larger ρ_d than the upper section, the above result is consistent with the magnitude relation of the secant stiffness. Additionally, a smaller S_r and larger ρ_d tends to increase the difference in the secant stiffness of the upper and lower sections, and the curve of the overall average of the specimens is located between the upper and lower sections. This suggests that the secant stiffness of the overall average is a composite of both series when the magnitude of the secant stiffness in the upper and lower sections of the specimen are different. This is further discussed based on the E_0 data presented in Section 4.3.

Fig. 7 shows an example of the stress–strain relationship of a specimen compacted in the field. Similar to Fig. 6, the secant stiffness before the peak in the upper

section is significantly smaller than that in the lower section although q of each curve approximately coincides at $\varepsilon_v = 1.5\%$. Moreover, because the ρ_d in the upper section of the specimen is higher than that in the lower section, the field-compacted specimen result is not consistent with the magnitude relationship of the secant stiffness. Tomita et al. (2021) attributed this to the disturbance caused by the shear failure of the compaction surface layer during field compaction. Furthermore, the overall average of the specimen is located between the upper and lower sections, which is similar to the behaviour of the upper section until approximately $\varepsilon_v = 0.3\%$.

4.2. Initial Young's modulus

Fig. 8 shows the relationships between the initial Young's modulus E_0 ($\Delta\varepsilon_v \approx 0.001\%$) and the ρ_d for the upper section, lower section, and overall averages of the specimens compacted in the laboratory. After compaction, the S_r was parameterised as 15–30%, 30–60%, and 60–80%. As described by Tomita et al. (2021), the E_0 increased with ρ_d; however, the entire data were affected by the S_r at the end of the compaction of the fill material. Moreover, some specimens have different E_0 under the same ρ_d because their S_r are different.

Based on the E_0 relation between the upper and lower sections of the specimen and overall average, the initial Young's modulus $(E_0)_{ave}$ was approximately halfway between the upper and lower sections. This result is observed regardless of the ρ_d or S_r.

Fig. 9 shows the relationships between the E_0 and ρ_d for the upper section, lower section, and overall averages of the field-compacted specimens. As shown in Fig. 8, the plotted data represent the S_r-specific compaction parameters. In general, the E_0 increases with the ρ_d and is affected by the S_r after compaction, similar to the compacted specimen in the laboratory. Based on a comparison of the upper and lower sections of each specimen, the E_0 of the upper section of the specimen, which has a higher ρ_d, was smaller than that of the lower section. This tendency was particularly evident in specimen groups with low S_r values. This might be because the disturbance at the upper section of the specimen shown in Fig. 7 occurred at the time of compaction, and the closer the S_r at the end of compaction was to the optimum degree of saturation, the less prominent the effect.

Most of the $(E)_{ave}$ points in the plotted data were located halfway between the upper and lower sections of the specimen. Additionally, the difference in E_0 between the upper and lower sections of the specimens was significant. This implies that it is difficult to appropriately evaluate the deformation characteristics of nonuniform specimens when evaluating the $(E_0)_{ave}$ of the overall average specimen.

Fig. 10 shows the relationship between the E_0 and ρ_d at the upper and lower sections of the specimens compacted in the field and laboratory. As shown in Fig. 8, the plotted data represent the S_r-specific compaction parameters. In addition, the upper section of the specimen compacted in the field, which was affected by disturbance at the time of field compaction, was plotted
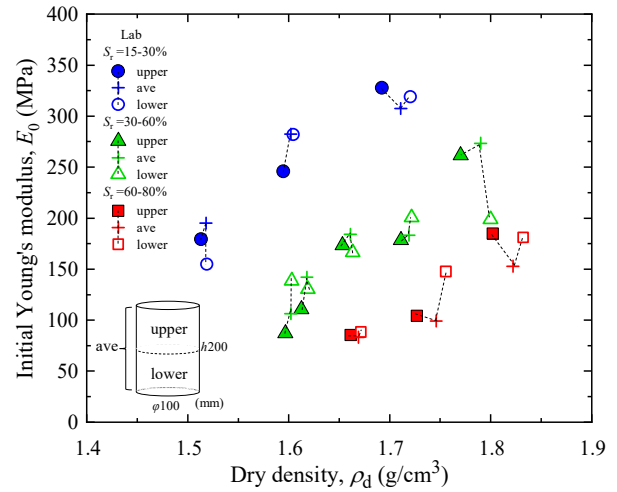
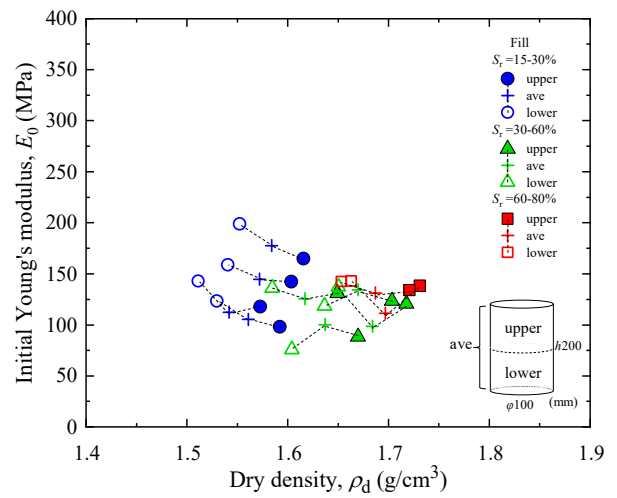**Figure 8.** E_0. vs ρ_d in laboratory-compacted specimens.

Figure 9. E_0. vs ρ_d in field-compacted specimens.

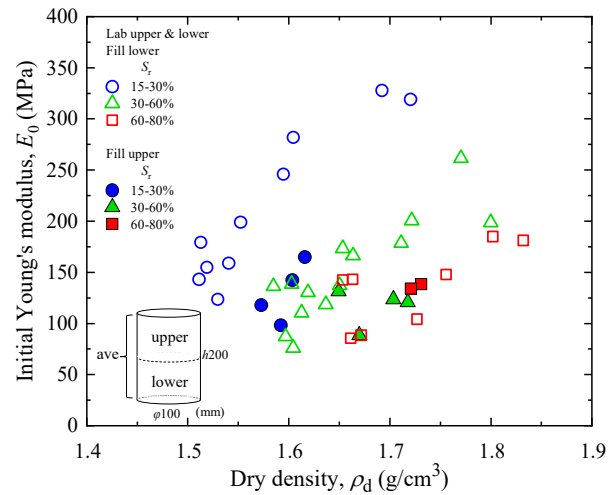**Figure 10.** E_0. vs ρ_d in laboratory and field-compacted specimens.

as filled data; whereas the lower section of the field-compacted specimen and upper and lower sections of the specimen compacted in the laboratory were plotted as open data. In general, E_0 shows a similar tendency in the upper and lower sections of the laboratory-compacted specimen and lower section of the field-compacted

specimen under the influence of the S_r and ρ_d after compaction. Meanwhile, for the same ρ_d, the upper section of the field-compacted specimen has a lower E_0 owing to the disturbance received during compaction compared to the data less affected by disturbance; and this difference is particularly evident in groups between 15% and 30%, where the S_r after compaction is lower. This implies that the reduction in E_0 owing to disturbance is affected by the S_r at the time of compaction. Hence, the $(E_0)_{ave}$ of the overall average specimen compacted in the field cannot be used to comprehensively evaluate the deformation characteristics of the nonuniform specimens.

4.3. Effect of non-uniformity on the initial Young's modulus

When the physical properties of the upper and lower sections of the specimen significantly differ because of the compaction method used, the comprehensive evaluation of the deformation characteristics of the compacted soil by measuring the $(E_0)_{ave}$, as shown in 4.1 and 4.2, is difficult. In this section, we focus on the local E_0 obtained from the test results and difference in the $(E_0)_{ave}$, and examine the conditions of the specimens that require an analysis of the local deformation.

The difference in the E_0 between the upper and lower sections of the specimen was evaluated by combining them in series using Eq. (1), which is based on Hooke's law:

$$(E_0)_{combined} = 2/\left[1/(E_0)_{upper} + 1/(E_0)_{lower}\right] \quad (1)$$

Here, $(E_0)_{combined}$ is the initial Young's modulus, $(E_0)_{upper}$ is the local initial Young's modulus in the upper section of the specimen, and $(E_0)_{lower}$ is the local initial Young's modulus in the lower section of the specimen.

Fig. 11 shows the relationship between the $(E_0)_{combined}$ obtained using Eq. (1) and measured $(E_0)_{ave}$. Here, the relatively-uniform laboratory-compacted specimens and non-uniform field-compacted specimens with an S_r gradient, ρ_d, and disturbance in the surface layer, are plotted. The data corresponding to the auxiliary line indicated by 1:1 indicates that the $(E_0)_{combined}$ and $(E_0)_{ave}$ are consistent.

The data shown in the plot are generally distributed along the auxiliary line, and the difference between the laboratory- and field-compacted specimens is insignificant. This indicates that the assumptions in Eq. (1) holds, and the relationship between the local and overall deformations can be expressed using this method without relying on the compaction method.

By arranging the 21 data points of $(E_0)_{combined}/(E_0)_{ave}$ - 1, the average value $\mu = 0.027$ and standard deviation $\sigma = 0.116$. $\mu \pm \sigma$ are obtained, as shown in the auxiliary line in Fig. 11. Furthermore, most of the plotted data, including measurement errors, were within 12 %.

Fig. 12 shows the $E_0/(E_0)_{ave}$-1 to $[\rho_d/(\rho_d)_{ave}$-1] relationship between the upper and lower sections of the laboratory- and field-compacted specimens, respectively. Here, $[\rho_d/(\rho_d)_{ave}$-1] on the horizontal axis shows the relative deviation of the ρ_d at the upper and lower sections of the specimen to the $(\rho_d)_{ave}$ shown in Table 1, where the
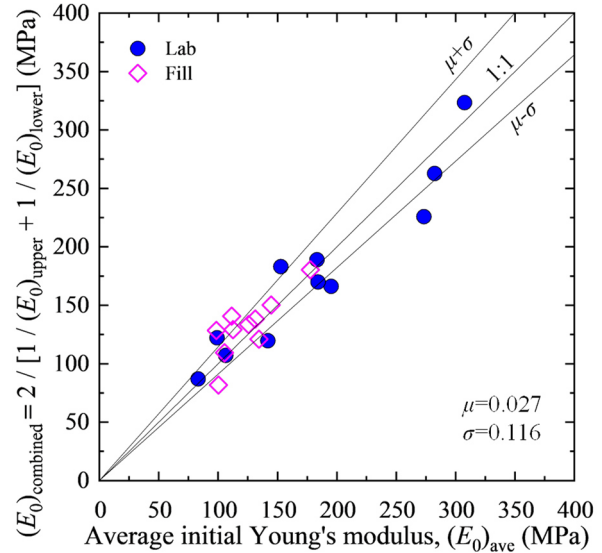

Figure 11. Relationships between the $(E_0)_{combined}$ at upper and lower sections of the specimen, and measured $(E_0)_{ave}$ of the entire specimen.
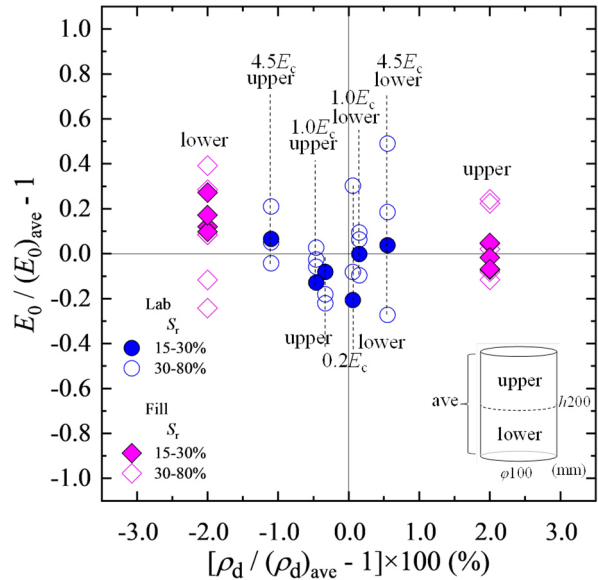

Figure 12. Relationships between $E_0 / (E_0)_{ave}$ - 1 and $[\rho_d / (\rho_d)_{ave}$ - 1].

absolute value increases because the specimen is non-uniform and the ρ_d gradient is large. In addition, an $E_0/(E_0)_{ave}$-1 value (on the vertical axis) of approximately 0 imply that the E_0 at the upper or lower section of the specimen is closer to the $(E_0)_{ave}$. As explained in Section 4.2, because the E_0 is affected by the S_r after compaction, the plots within 15–30% of the S_r after compaction are shown as filled data, whereas those within 30–80% of the S_r are shown as open data.

In general, the $E_0/(E_0)_{ave}$ - 1 of the compacted specimen in the field, which has a higher $[\rho_d/(\rho_d)_{ave}$ - 1] value, features a larger distribution width. The large distribution width is due to the difference in the S_r after compaction; however, the filled plot with S_r ranging between 15% and 30% was prioritised.

The $E_0/(E_0)_{ave}$ - 1 values of the laboratory-compacted specimen was distributed between -0.2 and 0.1 in both the upper and lower sections of the specimen, that is, relatively near 0, which is similar to the trend in the

$(E_0)_{ave}$. At S_r values ranging from 30% to 80% after compaction, the scatter ranged from -0.3 to 0.5, as indicated in the lower sections of the data at a compaction energy level of $4.5E_c$. As the compaction energy level increased to $4.5E_c$, the ρ_d gradient of the laboratory-compacted specimen increased, and the dispersion of physical properties due to the preparation method further intensified, thereby resulting in a difference between the E_0 and $(E_0)_{ave}$.

Meanwhile, the $E_0/(E_0)_{ave}$ - 1 values at the upper section of the field-compacted specimen with an S_r of 15–30% after compaction was approximately 0, which is similar to the trend in the $(E_0)_{ave}$. This is because the ρ_d at the upper section of the field-compacted specimen is relatively high, and the E_0 reduces owing to the effect of disturbance. In addition, the values of $E_0/(E_0)_{ave}$ - 1 at the lower section of the field-compacted specimen are slightly higher (0.1–0.3). This is because the $(E_0)_{ave}$ was reduced by the disturbance in the upper section of the specimen, and the value in the lower section of the specimen with a negligible effect due to disturbance is relatively high. Based on Fig. 10, the locally-measured E_0 of the lower section of the field-compacted specimen was affected by the S_r and ρ_d after compaction; moreover, its trend is similar to that of the laboratory-compacted specimen. However, the conventional $(E_0)_{ave}$ indicated a minimum value of 20% owing to the effect of the low-stiffness section of the surface layer during field compaction.

5. Conclusions

To conveniently evaluate the deformation characteristics of field- and laboratory-compacted non-uniform specimens in the vertical depth direction, the authors attempted to separate and evaluate the upper and lower sections of the specimens using small local displacement transducers. The following conclusions were drawn:

Although the field- and laboratory-compacted specimens exhibited different degrees of compaction, the compaction was non-uniform and the difference in their deformation characteristics could be evaluated by separately evaluating the deformation characteristics of the upper and lower sections of the specimen using small local displacement transducers. Moreover, the $(E_0)_{combined}$ value based on the E_0 of both specimens is consistent with the average $(E_0)_{ave}$.

For the specimen compacted in the laboratory using a compaction rammer, the dry density ρ_d of the specimen was relatively uniformly distributed provided that the compaction energy level was $0.2E_c$ or $1.0E_c$. Additionally, the difference between the $(E_0)_{ave}$ of the specimen obtained using the conventional triaxial compression test and local E_0 obtained using the local strain measurements at the upper and lower sections of the specimen was negligible. However, when the compaction energy level was $4.5E_c$, variations in the physical properties and initial Young's modulus occurred because of the different specimen fabrication methods.

In addition, the non-uniform ρ_d of the field-compacted specimen and presence of the low-stiffness section at the top of the field-compacted specimen owing to the disturbance of the surface layer during compaction significantly affected the local E_0 and total $(E_0)_{ave}$ of the field-compacted specimen. Therefore, compared with the laboratory-compacted soil, when the E_0 is evaluated against the average of the entire specimen, the field-compacted soil indicated an $(E_0)_{ave}$ that is up to 20% lesser, which is similar to that of the conventional method; this is because it is affected by the local low-stiffness section near the surface layer. This result suggests that evaluations using the non-destructive inspection of the surface layer may result in underestimations compared with the stiffness obtained from laboratory-compacted soil because field-compacted soil has a local low-stiffness section near the surface layer.

References

Goto, S., Tatsuoka, F., Shibuya, S., Kim-Y.-S., Sato, T. 1991. "A simple gauge for local small strain measurements in the laboratory", *Soils Found.*, 31(1), pp. 169-180. https://doi.org/10.3208/sandf1972.31.169

Heitor, A., Indraratna, B., Rujikiatkamjorn, C. 2016. "Small strain behavior of compacted subgrade soil", *The 3rd International Conference on Transportation Geotechnics (ICTG2016)*, Portugal, pp. 260-267. https://doi.org/10.1016/j.proeng.2016.06.033

Moony, M. A., Adam, D. 2007. "Vibratory roller integrated measurement of earthwork compaction: an Overview", *7th International Symposium on Field Measurements in Geomechanics 2007*, the United States, pp. 1-12. https://doi.org/10.1061/40940(307)80

Sasaki, T., Kawamura, S., Koseki, J. 2021. "Liquefaction properties of two types of sandy soil specimens with different compaction thickness", *GeoChina 2021: Advances in Innovative Geotechnical Engineering*, China, pp. 19-30.

Tatsuoka, F., Hashimoto, T., Tateyama, K. 2021. "Soil stiffness as a function of dry density and the degree of saturation for compaction control", *Soils Found.*, 61, pp. 989-1002. https://doi.org/10.1016/j.sandf.2021.06.007

Thomson, P.R., Wong, R.C.K. 2008. "Specimen nonuniformities in water-pluviated and moist-tamped sands under undrained triaxial compression and extension", *Can. Geotech. J.*, 45(7), pp. 939-956. https://doi.org/10.1139/T08-023

Tomita, Y., Koseki, J., Tatsuoka, F. 2021. "Evaluation of non-uniformity of sandy soil specimens compacted in the field and in the laboratory and its effect on strength and deformation characteristics", *Jpn. Geotech. J.*, 6(4), pp. 355-369 (in Japanese). https://doi.org/10.3208/jgs.16.355

Tomita, Y., Koseki, J., Tatsuoka, F. 2022. "Empirical equations expressing the effects of several factors on the strength-deformation characteristics of in-situ compacted sandy soil", *J. Japan Soc. Civ. Eng., Ser.C (Geosph. Eng.)*, 78(3), pp. 197-209 (in Japanese). https://doi.org/10.2208/jscejge.78.3_197

Zhao, C., Koseki, J. Sasaki, T. 2018. "Image based local deformation measurement of saturated sand specimen in undrained cyclic triaxial tests", *Soils Found.*, 58, pp. 1313-1325. https://doi.org/10.1016/j.sandf.2018.07.008